MAGNETOHYDRODYNAMIC GENERATOR EXPERIMENTAL STUDIES

FINAL TECHNICAL REPORT

EDWARD S. PIERSON

JUNE 12, 1972

PREPARED FOR THE JET PROPULSION LABORATORY

UNDER CONTRACT NO. 952985

DEPARTMENT OF ENERGY ENGINEERING
UNIVERSITY OF ILLINOIS AT CHICAGO CIRCLE
CHICAGO, ILLINOIS 60680

MAGNETOHYDRODYNAMIC GENERATOR EXPERIMENTAL STUDIES

FINAL TECHNICAL REPORT

EDWARD S. PIERSON

JUNE 12, 1972

PREPARED FOR THE JET PROPULSION LABORATORY

UNDER CONTRACT NO. 952985

THIS WORK WAS PERFORMED FOR THE JET PROPULSION LABORATORY, CALIFORNIA INSTITUE OF TECHNOLOGY, AS SPONSORED BY THE NATIONAL AERONAUTICS AND SPACE ADMINISTRATION UNDER CONTRACT NAS7-100.

DEPARTMENT OF ENERGY ENGINEERING
UNIVERSITY OF ILLINOIS AT CHICAGO CIRCLE
CHICAGO, ILLINOIS 60680

ACKNOWLEDGEMENT

The use of the facilities at Argonne National Laboratory is gratefully acknowledged, along with the advice and encouragement of Dr. M. Petrick of Argonne National Laboratory and Dr. D.G. Elliott of Jet Propulsion Laboratory. E.M. Spleha did most of the mechanical design; R.A. Esposito, L.M. Indykiewicz, and J.J. Reed aided in the construction and operation; and M.A. Brown, J.B. Alwin, and S.C. Lin aided in the computations.

Construction of much of the generator and facility was supported by the U.S. Air Force under Contract F33615-67-C-1375 with the Air Force Aero Propulsion Laboratory, Wright-Patterson Air Force Base, Ohio.

ABSTRACT

The results for an experimental study of a one-wavelength MHD induction generator operating on a liquid flow are presented. First the design philosophy and the experimental generator design are summarized, including a description of the flow loop and instrumentation. Next a Fourier series method of treating the fact that the magnetic flux density produced by the stator is not a pure traveling sinusoid is described and some results summarized. This approach appears to be of interest after revisions are made, but the initial results are not accurate. Finally, some of the experimental data is summarized for various methods of excitation.

TABLE OF CONTENTS

SECTION I

INTRODUCTION

The successful development of the MHD induction generator depends on the selection of a compromise between electrical and viscous losses such that an acceptable efficiency is obtained. Thus the basic objective of the program is to gain further understanding of the generator and of the associated losses. Particular emphasis has been placed on the divergence between the anticipated and measured performances at low slips. The philosophy was to design a generator and test facility with the maximum amount of flexibility and instrumentation. Steady operation was desired, and obtained for periods of up to a day.

A one-wavelength-long generator geometry was selected as this appears to be the only feasible choice except for the largest sizes. This naturally lead to the primary emphasis being on the study of end losses and compensating methods. Provision has been made for removable compensating poles, grading of the traveling-field winding, and the use of both vaned and unvaned channels outside of the traveling-field region. This allows the comparison of all cases while utilizing the same traveling-field structure.

Over 200 data points have been measured for the experimental generator under a variety of operating conditions with the unvaned channel. These include:

1. Uncompensated, connected to the power line.
2. Uncompensated, connected to the power line, end coils shorted to reduce the effect of the open magnetic circuit.
3. Uncompensated and self-excited for both cases above over a frequency range of about 35 to 60 hertz.
4. Uncompensated, two-wavelength-long field connection.
5. Compensating poles excited, connected to the power line.
6. Compensating poles excited, self-excited over a frequency range of 37 to 53 hertz.
7. Harmonic measurements and tests of system accidents.

The data runs with the compensating poles have been limited (40 points) due to difficulties in properly setting the compensating-pole currents, as different criteria (maximum power, phase balance) lead to different operating points.

In Section II the design philosophy, the experimental generator, and the facility are briefly presented. The design is described in more detail in a previous report [1]*, which also includes a summary of the theory. The initial Fourier-series model for the MHD induction generator is presented in Section III. The experimental results are summarized in Section IV.

---

* Numbers in brackets references at the end of the report.

SECTION II

EXPERIMENTAL GENERATOR AND FACILITY

2.1 DESIGN PHILOSOPHY

The basic objective of this experimental program is to gain further understanding of the operation of the MHD induction generator, and in particular to examine the discrepancies between the expected and the actual performances at low slips. To this end it is desired:

1. To build a machine whose performance can be accurately predicted.
2. To do a careful, controlled experiment capable of steady operation.
3. To design a generator capable of reaching a high enough slip, say $s = -0.8$ as shown by previous experiments [2], so that the losses which cause the discrepancies at small slips are not significant.
4. To build a one-wavelength generator as this appears to be best for space applications. The longer wavelength of the one-wavelength machine yields a stronger interaction between the fluid and the traveling field and a better power factor. More than one slot per phase per pole should be used to obtain a better traveling magnetic field and to allow operation as both a single - and a multi-wavelength machine by reconnecting the coils.
5. To include provisions for a careful study of the end losses. The machine must be capable of operation with and without both compensating poles and vanes in the end regions.
6. To wind the exciting coils in such a fashion that the current in each slot can be independently controlled, allowing grading of the winding for end studies and balancing the phases. This is accomplished by winding each coil around the back of the core so that each coil is in only one slot, and by including a tap in each coil.
7. To build a machine that is capable of self-excited operation as a generator. This is not only necessary for a practical machine but, lacking a variable-frequency power source, it allows greater experimental flexibility. It should also be capable of operation from a 60-hertz three-phase power line.
8. To include provision for operation with a two-phase (liquid and vapor) mixture as this is expected for practical power systems.

These above points formed the basic framework for this generator design.

To achieve the above major points, and to obtain the maximum amount of information from a single traveling-field structure or stator, a constant-field and fluid-velocity generator was chosen as this has more experimental flexibility than the variable-fluid-velocity generator with either constant or varying field velocity. More, important, the variable-velocity machine would not yield the controlled experiment desired because of the

interaction between the end and variable-velocity effects. It was felt that the major areas where information was required were end losses and operation with two-phase working fluids, and that it was preferrable to concentrate on points 1, 5, and 8 and leave variable field velocity for later experiments.

2.2. EXPERIMENTAL GENERATOR DESIGN

The main constraint on the size of the generator is the flow loop, and in particular the rating of the pump, 250 gallons per minute at 82 psi. The generator is designed to use the full flow capacity of the pump only at the highest desired fluid velocity (slip), and to allow leeway for pressure losses in the flow loop, the pressure wasted as lost kinetic energy into the supply tank, and the uncertainty in the actual pump performance.

The electrical constraints on the experimental generator are very loose. Three-phase, 60 hertz, 480 volt power is available with more than adequate capacity. The generator is driven through three single-phase variacs for control. Capacitors in parallel with the generator are used to reduce the reactive power load on the variacs, and are required for self-excited operation. Operation at other frequencies is possible self-excited.

The practical constraints for obtaining an acceptable experimental performance are more subtle. Some of these were mentioned in Section 2.1. Further constraints are:

1. The viscous pressure drop must represent a small fraction of the total available pressure in order to model a practical generator. This is required both for acceptable efficiency and for a large field-fluid interaction where the electromagnetic force dominates over the viscous force. Otherwise a sharp Hartmann profile (or the equivalent for turbulent flow) will not be attained, and the ohmic losses in the boundary layers will be unreasonably large [3].
2. The generator height parallel to the magnetic field, $2a_f$, should be small to reduce the exciting ampere turns and power required, but large to reduce the viscous loss. Also, a_f has to be larger than the wall and/or insulation thickness so that most of the field volume performs useful work, inproving the power density and power factor. Finally, $2\pi a_f/\lambda \ll 1$, slit-channel model, for an acceptable power density, where λ is the wavelength.
3. The wavelength should be long for a strong field-fluid interaction, but short to reduce the viscous loss. The wavelength determines the room available for the exciting winding, and thus the number ampere turns and slots per phase per pole.
4. The generator width c should be large so that the effects of the cooper side walls and the current loops closing through them are small, but increasing the width decreases the fluid velocity and thus the wavelength.

5. The stator design should be such as to minimize the effect of slot harmonics, which appear to have been important in previous experiments [4]. The design should allow their effects to be observed experimentally.
6. Conducting channel walls should be avoided because their ohmic loss will be proportionally very large in a small generator (smaller ratio of generator volume to surface area). Also, the walls will be more sensitive to slot harmonics, which decrease away from the edge of the core. In order to avoid wall loss dominating the generator performance, hiding the very losses of interest in this experiment, and interfering with self-excited operation; it was decided to use a non-conducting fluid channel except for copper side bars to reduce the edge effects.

As can be seen from the above, the design of the experimental generator is not a trivial exercise because many of the constraints are contradictory.

2.2.1 Channel Design and Dimensions

A fluid channel is required to protect the stator and reduce the danger of leakage but, as mentioned, conducting channel walls should be avoided. Thus, it was decided to use a fiberglass channel because fiberglass is flexible and has a higher temperature rating (compared to lucite). The minimum wall thickness a_i, 1/16 inch to avoid the danger of breakage, is chosen to minimize the required exciting ampere turns. It is assumed that the iron core is perfectly smooth and is used to mechanically back up the channel and absorb all of the pressure force. (The channel was tested at the maximum working pressure of 100 psi before its use with NaK). Incidently, the core will probably be similarily used for structural backup in a power system.

In spite of the insulating top and bottom channel walls, conducting side walls are desired to facilitate the closing of the fluid current loops and thus increase the power density. This is accomplished by using cooper side walls, as shown in Fig. 1. The copper bars are clamped so that they cannot be pushed out by the static pressure force, and have a lip which rests against the core so that they cannot be pulled into the channel by the $\vec{J} \times \vec{B}$ force or the dynamic pressure force. Leakage between the copper and the fiberglass is prevented by inserting the fiberglass into a slot in the copper. The copper extends into the region between the two cores, in spite of slightly increased ohmic losses, to provide additional sealing and the mechanical strength to support the cores when they are clamped together.

The first dimension chosen was the height $a_f = 0.25$ cm, compared to the wall thickness of 0.159 cm. The choices for λ and s_{max}, the maximum attainable slip, are independent but together fix the other parameters and the generator performance. The relevant equations

are $v_{max} = (1 - s_{max})f\lambda$, and $c = Q_{max}/2a_f v_{max}$ where f is 60 hertz and Q_{max} is the mixiumum flow rate of the pump. After several trials, the values $\lambda = 0.21$ m and $s_{max} = -0.8$ were selected, giving $c = 0.1393$ m. (In the actual generator c turned out to be about 0.1405 m because it was not feasible to control the width of the iron core precisely.)

The estimated power and pressure drops for this design are shown in Table I, where the equations for the slit-channel induction machine were used [3, 5] with the design peak magnetic flux density $B = 0.4$ wb/m^2 and the appropriate NaK properties of $\sigma_f = 2.38 \times 10^6$ mhos/m, $\rho = 847$ kg/m^3, and $\eta = 4.68 \times 10^{-4}$ kg/m-sec. Only the traveling-field region is considered, perfect compensation for the ends is assumed, and the edge effects are ignored. In the table P_s is the power supplied by the fluid to the exciting winding (electrical output power when coil and core losses are ignored), P_m is the mechanical input power, Δp_{em} is the electromagnetic pressure difference, and R_e is the Reynolds number. The viscous pressure drop Δp_v is calculated using the friction factor for turbulent flow without a magnetic field [6] as the case with a magnetic field is not clearly documented [3].

The correction required for the non-flat velocity profile is shown in Table II. The Hartmann number M based on the rms magnetic flux density is 50.4, which is on the borderline of being too small. To see this, the ratio of δ^*, the distance the channel wall would have to be moved in to maintain the same volume flow rate if the velocity was constant at the maximum (center line)value, to a_f is calculated using an approximate turbulent boundary-layer solution [3]. Since for a Hartmann profile $\delta^*/a_f = 1/M$, this is used tocalculate an effective M, M_{eff}, as far as the fluid ohmic losses due to the non-flat profile are concerned. The effect of this is to multiply P_m by the profile factor F_m, which takes the extra ohmic losses into account, but to leave P_s unchanged [3]. The increase in P_m is 7% at s_{max}, with larger increases as s approaches zero.

One other point is to estimate the effect of the copper side walls or the finite generator width on the performance. The peak current in the side walls, assuming that all of the fluid current flows in them and that their presence does not change the fluid current from the infinite-width value, is 2210 amps for $s = -0.8$, giving an ohmic loss for both sides of 465 watts which is limited by the skin depth of the copper. The ratio of this ohmic loss to that in the fluid, neglecting the profile factor, is 0.163 for this generator independent of the slip, so that the power density in the generator will be decreased. This is an upper limit, in practice the fluid current constraints should reduce substantially the ohmic loss in the copper.

2.2.2. Traveling-Field Structure

The purpose of the traveling-field structure or stator is to produce the required magnetic field with the minimum of distortion from a pure traveling sinusoid. The effect of distortion is to generate spatial harmonics with a shorter wavelength and slower field velocity, and consequently to reduce the efficiency due to the increased ohmic losses in the fluid. Distortion is created by many sources, the most important being

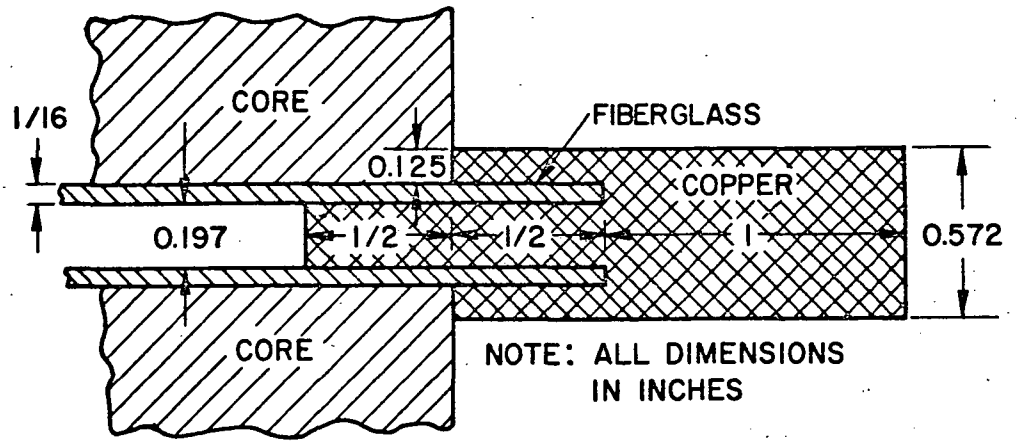

Fig. 1 Detail of channel construction.

TABLE I. Powers and pressure drops for the traveling-wave region.

Parameter	Units			
s		-0.8	-0.5	-0.3
v	m/sec	22.7	18.9	16.4
B	wb/m^2	0.4	0.4	0.4
P_s	watts	3570	2230	1340
P_m	watts	6420	3350	1740
Δp_{em}	psi	59.1	36.9	22.2
R_e		3.96×10^5	3.30×10^5	2.86×10^5
Δp_v	psi	9.4	6.8	5.2
Δp_{total}	psi	68.5	43.7	27.4

TABLE II. Velocity profile corrections, M = 50.4.

Parameter			
s	-0.8	-0.5	-0.3
R_e	3.96×10^5	3.30×10^5	2.86×10^5
δ^*/a_f	0.062	0.056	0.05
M_{eff}	16.1	17.9	20
F_m	1.069	1.084	1.108

the slots in the iron structure for the winding, the use of a finite and small number of phases with pulsed rather than sinusoidal turns densities, and saturation of the iron. To minimize these effects, the following design ideas were adopted:

1. The two stator cores were designed so that they can be operated with tooth opposite tooth or with tooth opposite slot in order to reduce slot harmonic effects and study them experimentally. This is accomplished by making the two end teeth of different widths so that reversing one core relative to the other switches cases. The core lamination dimensions are shown in Fig. 2, and the experimental fields produced by the two cases are compared in Reference 1. Also, short straight sections are provided at the end of each slot to allow the possible later insertion of highly-permeable slot plugs which would smooth out the air-gap magnetic field at the price of increased leakage flux.

2. More than one slot per phase per pole or else more than three phases, either of which requires more slots per wavelength, were used, and this results in a smoother field as explained previously [1].

3. The width of the slot (or tooth) was tapered so that more iron area is available where needed to handle the leakage flux without saturation.

The traveling-field-structure design is only summarized here, as it is presented in detail in Reference 1. In the experimental generator there was only room for 12 slots. The number of ampere turns was calculated to be 1230 per slot at s = -0.8, the maximum case, including the Carter coefficient and a small allowance for iron reluctance. Each coil consists of 45 turns made out of three #14 wires in parallel in the slot butt-soldered to a rectangular bar of about twice the copper area outside the slot. The coil loss was estimated to be 440 watts for this case using an assumed effective copper area of 0.7 and a larger copper area outside of the slot. (This is low because the effective area was off, and will be increased to about 700 watts.) The core loss for the Armco electrical steel M-14 was estimated to be 92 watts including the lamination packing factor.

One important point in the stator design is to build in adequate monitoring devices. Two types are required - thermocouples to measure the coil temperatures at various locations in the slots and in the loop around the back of the core, and coils to monitor the field. There are 19 two-turn magnetic-field monitoring coils on each core, located as shown in Fig. 2. The locations were chosen to observe the field in the core above the slots, which includes the compensating flux (see the next section); the flux through some of the teeth, including the leakage flux; the flux through some of the slots; and the flux entering the air gap. They will be useful in evaluating the stator design and in monitoring the operation with fluid present in the channel since then the field cannot be directly measured.

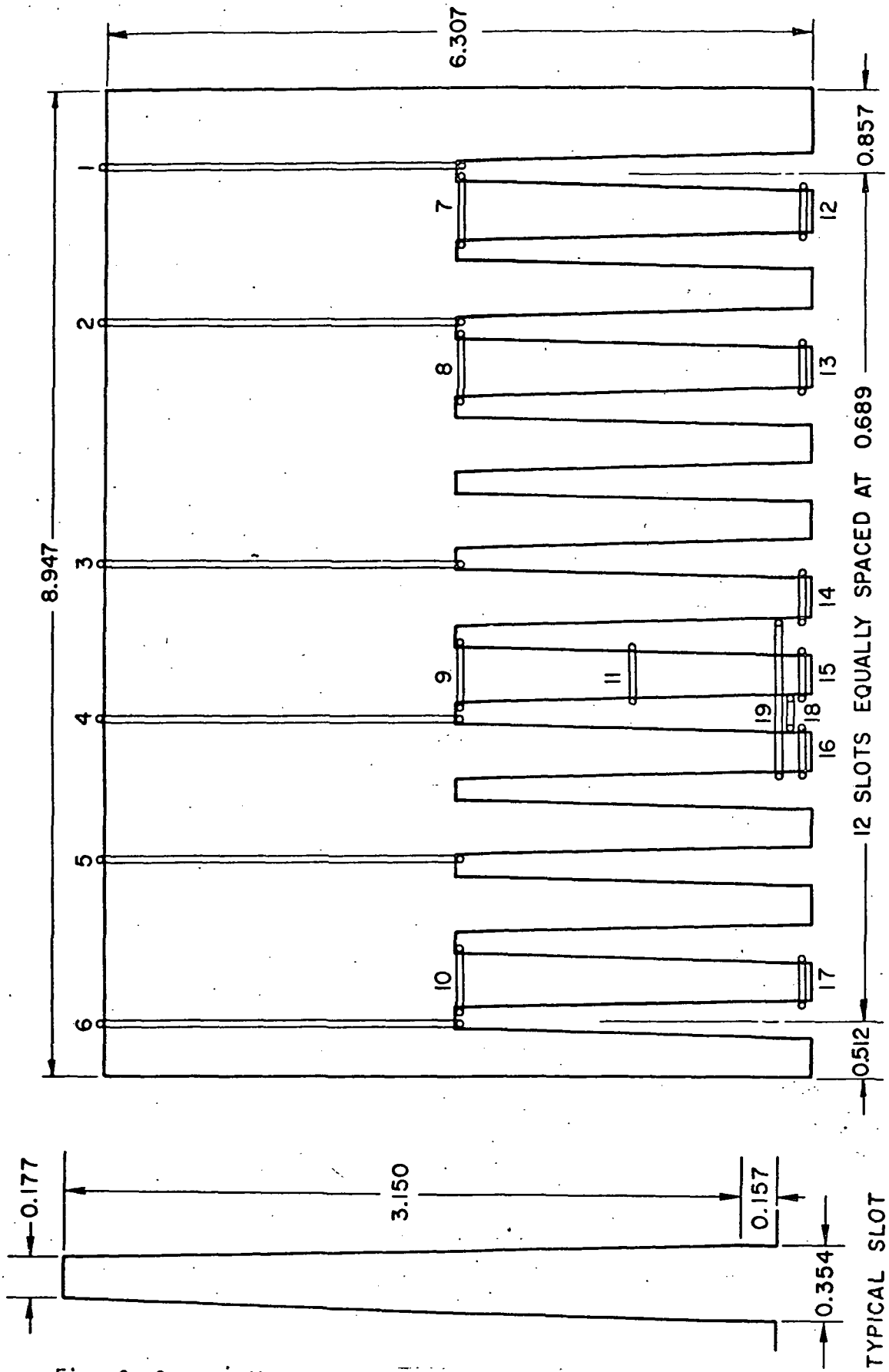

Fig. 2 Stator dimensions and magnetic-field monitoring-coil locations.

2.2.3 Compensating Poles

In the regions where the fluid enters and leaves the traveling magnetic field undesired voltages and currents are induced in the fluid, and these cause increased ohmic losses. In order to set up the proper boundary conditions so that the traveling-field region acts like a segment out of an infinitely-long machine, Elliot proposed the use of compensation poles [7]. The peak magnetic flux density B_c and length L_c must satisfy $B_c L_c = B\lambda/2\pi$ assuming a slit-channel machine. Arbitrarily choosing L_c to be one inch gives $B_c = 0.525$ wb/m^2. The channel wall thickness under the compensating poles was increased to 1/8-inch to give a stronger structure because the poles are removable. Then, 2380 ampere turns is required for each of the four pole structures, and 85 turns with a tap at 70 turns are on each pole. Excitation is by means of the phase voltages rather than the phase currents because this tends to be self-compensating for the phase shift required as the fluid reaction field varies. (This is discussed in Reference 1.)

Insulating vanes in the channel under the compensating poles are required to reduce the ohmic loss, but at the penalty of increased viscous loss. It is necessary to calculate (or estimate) both losses as a function of the number of vanes and optimize. The viscous loss is easily calculated using the available hydrodynamic equations, but the ohmic loss can only be crudely estimated. Using the results of Moszynski [8] to estimate the ohmic loss, a compromise of six vanes was selected.

2.2.4 Discussion

The results of the previous calculations are summarized in Table III to give a tentative idea of the performance to be expected at three values of slip. All of the losses are considered, except that the field harmonics are not included and perfect end compensation is assumed. The effect of the copper side bars is to reduce the fluid current and thus the power density. This effect is estimated by assuming that the induced electric field or voltage in the fluid stays constant since the magnetic flux density is assumed to be constant. (This means that the sum of the ohmic losses in the fluid plus the side bars decreases as the bar conductivity decreases.) The ratio of the ohmic loss in the side bars to that in the fluid neglecting the velocity profile correction is defined as β, where $\beta = 0.163$ for this generator from Section 2.2.1. Then the ratio of the equivalent resistances of the two regions is also β, and the fluid current is multiplied by $1/(1+\beta)$ for the same induced voltage. Finally, the generated power in the fluid, which depends on $\vec{E}\cdot\vec{J}$, is $P_s/(1+\beta)$; where P_s is the power without the side bar correction, Table I. The mechanical input power modified for the side bar correction is P_m'.

The separate power losses are also included in Table III. The ohmic loss in the exciting winding is based on the measured DC coil resistances. The reduction in the fluid currents due to the bars also appears here because the reaction field and thus the required ampere turns are reduced.

Table III. Summary of theoretical generator performance.

Paramenter	Units			
s		-0.8	-0.5	-0.3
$[1/(1+\beta)]P_s$	watts	3070	1920	1150
P_e	watts	640	590	560
P_{core}	watts	90	90	90
P_{cp}	watts	230	230	230
P_{out}	watts	2110	1010	270
P'_m/P_s		1.67	1.42	1.26
P'_m	watts	5980	3160	1680
Δp_{em}	psi	55.0	34.8	21.4
Δp_v	psi	9.4	6.8	5.2
Δp_{cp}	psi	10.8	7.5	5.6
Δp_{tot}	psi	75.2	49.1	32.2
P_{in}	watts	8190	4460	2530
e_g		0.26	0.23	0.11

This is taken into account by multiplying sR_{Mf} by $1/(1 + \beta)$, and amounts to decreases in excitation loss of 15%, 8%, and 3% for s = -0.8, -0.5, and -0.3. The core loss, P_{core}, is essentially independent of slip or the side or the side bar effect except for the slight change in the leakage flux which is ignored. The excitation power for the compensating poles, P_{cp}, depends only on the flux density which is independent of the slip. The net electrical output power is P_{out}.

Similarly, the mechanical pressure drops are taken from the previous results. The electromagnetic term Δp_{em} comes from P'_m, and Δp_v is given in Table I. The pressure drop for the compensating poles, Δp_{cp}, is estimated by assuming that the electrical drop is equal to the viscous drop since the calculation for the electrical pressure difference was very rough. The net result is estimated efficiencies of 0.26 at s = -0.8, 0.23, at -0.5, and 0.11 at -0.3.

2.3 THE FLOW LOOP AND INSTRUMENTATION

The existing NaK-N_2 flow loop at the Argonne National Laboratory with the addition of a new extension intended specifically for the induction generator is used for these experiments. The pump, heat exchanger, supply tank, separation system, and part of the control system are utilized from the existing loop. The flow path is from the supply tank to the pump, the heat exchanger, then to the extension and generator, and back to the storage tank. For the two-phase experiments the supply tank also serves as the separator. There is an air-operated shunt or bypass valve between the pump outlet and the supply tank, but this valve is always closed for tests.

The pump, rated at 250 gpm at 220 ft. head, has a combined rotor-impeller assembly with a completely sealed or canned stator winding. A small portion of the pumped NaK is allowed to recirculate through the rotor cavity to cool the motor and lubricate the aluminum oxide hearings. This construction leads to a compact pump with no possiblity of leakage, but since it dumps nearly all of the motor ohmic loss into the NaK it may also cause an excessive temperature rise in the NaK. To maintain the NaK temperature below about 125°F, required for the fiberglass tests section, a stainless-steel finned-tube NaK-to-air heat exchanger is used. The cooling capacity is approximately 12 kilowatts at an outside air temperature of 75°F, a NaK inlet temperature of 150°F, and a flow rate of 100 gpm; but this is less than the power dumped into the NaK by the pump.

The extension for the induction generator tests contains a venturi coupled with a differential pressure transducer for measuring the NaK flow rate, a three-inch air-operated valve to control the pressure across the test section, and three-inch ball valves to isolate the extension from the rest of the loop and from the test region so that system changes can be easily made. The test region includes the mixer for adding nitrogen to the NaK flow and the fiberglass test section. The nitrogen supply will be obtained from a 42,500 ft^3

capacity trailer. The nitrogen is fed into the mixer through four check valves to prevent flow of the NaK back into the nitrogen system. The mixer consists of an 11-inch length of three-inch Schedule 10S stainless steel pipe with 900 1/8-inch diamerer holes enclosed by a concentric length of five-inch Schedule 40 pipe into which the nitrogen is introduced. The nitrogen flow will be measured with an orifice and a differential pressure transducer. It will also be necessary to measure the void fraction by means of a gamma-ray source and a scintillation photo-multiplier tube.

Pressure measurements in the test section are made by means of gauge-diaphragm seal assemblies. A 316 stainless steel diaphragm is welded to the upper chamber in a two-chamber, 316 stainless steel pot assembly. The upper chamber is connected to a gauge and/or a transducer by tubing and the upper assembly is filled with instrument oil. The gauge accuracy is 1/2% of full scale. The lower chamber of the diaphragm unit is connected to the test section and to a bleed system for purging. Five pressure taps are provided on one side of the channel with a spare set on the other side. The tap locations are at the entrance, exit, and center of the traveling-field region and the outer ends of the compensating poles.

SECTION III

AN INITIAL FOURIER-SERIES MODEL*

3.1 INTRODUCTION

Several different approaches have been utilized to develop analytical models for the MHD induction generator. Initially most studies were based either on field models using a single traveling magnetic field or on the techniques developed previously for rotating induction motors, such as circle diagrams. These were limited in their treatment of slot harmonics, fringing fields, fluid velocity profiles [3], etc. Slot harmonics, for example, can be minimized for rotating induction machines because the slots in the rotor can be skewed, but harmonic effects may be significant for linear induction machines. Recently two new approaches to linear induction machines have been proposed, and these can treat arbitrary current excitations and stator geometries. They are: (1) Elliott [9] analyzes the induction generator by breaking the stator winding and the fluid secondary into discrete pieces and then solving for the total current distribution and magnetic field using superposition and matrix techniques. (2) The Fourier-series method described below.

3.2 EMPTY-CHANNEL MAGNETIC FLUX DENSITY

The magnetic flux density with no fluid present is calculated in three steps for the tooth of one core opposite the slot of the other core. This is the only case studied experimentally with the fluid present. First the field due to the current in the coil sides in a pair of slots is determined and broken down into Fourier series components. A slit-channel model is used, that is the magnetic field is assumed to be completely transverse to the fluid velocity and to not vary over the transverse direction. The neglect of the transverse variation means that the alternate location of the coils and slots on either side of the air gap has no effect on the field. In addition, fringing at the ends of the stator (magnetic core) is neglected, the effect of slots in the stator iron is not considered at this point, and the iron is assumed to be infinitely permeable. Second, the total field is found by adding together the contributions from the currents in all 24 slots or coil sides, first for the eight per phase and then for the three phases. Finally the effect of the slots in the iron is included and the total magnetic field appropriately modified.

3.2.1. Magnetic Field Due to a Pair of Coil Sides

The magnetic flux density produced by a single coil located in a single slot is found from Ampere's law

$$\oint_C \frac{\vec{B}}{\mu}\cdot d\vec{\ell} = \int_S (\vec{J}\cdot\vec{n})\,da, \qquad (3.1)$$

* Based in part on a special project performed by M. A. Brown.

conservation of flux,

$$\oint_S (\vec{B}\cdot\vec{n})\,da = 0, \tag{3.2}$$

and the constituent relations for the iron and the air gap, where $\vec{B}$ is the magnetic flux density, $\vec{J}$ the current density, and μ the permeability. For a slit-channel model and infinitely permeable iron only the transverse flux density B has to be considered. With no magnetic fringing Eq. 3.2 simplifies to

$$\int_0^L B\,dx = 0, \tag{3.3}$$

where L is the length of the stator.

With no fluid present the slit-channel single-coil field has no spatial dependence except at the coil location where the field discontinuity is

$$\Delta B = \mu_o NI/g \tag{3.4}$$

for NI ampere-turns per coil (N turns carrying I amperes) and an air gap of g. The time dependence is contained in I, and the coil is assumed to have negligible width.

The field due to the combination of two coil sides located in slots a half wavelength apart is found from the jump and conservation conditions, Eqs. 3.4 and 3.3. The form of the field is a square wave with different amplitudes for the positive and negative excursions to preserve the zero-average value. The resulting Fourier series for the two coil sides is

$$B = \frac{\mu_o NI}{\pi g} \sum_{m=1}^{\infty} \left[C_m \cos(\xi m x) + D_m \sin(\xi m x)\right]; \tag{3.5}$$

where

$$C_m = \frac{1}{m}\left\{\sin\left[m\xi(d+n\delta)\right] - \sin\left[m\xi(d+(n+12)\delta)\right]\right\}, \tag{3.6}$$

$$D_m = \frac{1}{m}\left\{\cos\left[m\xi(d+(n+12)\delta)\right] - \cos\left[m\xi(d+n\delta)\right]\right\}, \tag{3.7}$$

$$\xi = 2\pi/L \tag{3.8}$$

is the wave number for the series, and n is the number of the first coil side under consideration ($0 \le n \le 11$). Here L, the stator length, is 8.947 inch and is made up of 24 slots spaced δ = 0.3445 inch apart and two oversized ends of length d = 0.512 inch. Note that ξ is not the same as the wave number $k = 2\pi/\lambda$ for the excitation winding due to the stator construction used.

An alternative approach to that used above is to determine the field due to each coil side independently. This allows the results to be easily

extended to include the compensating coil currents and methods of grading the excitation.

3.2.2 Magnetic Field Due to All Coil Sides

The exciting currents for the three-phase system are

$$I_A = I_a \cos(\omega t), \tag{3.9a}$$

$$I_B = I_b \cos(\omega t - \phi), \tag{3.9b}$$

and

$$I_C = I_c \cos(\omega t - \theta); \tag{3.9c}$$

where I_a, I_b and I_c are the amplitudes of the three currents and ϕ and θ are the phase angles for I_B and I_C relative to I_A. For a balanced three-phase excitation the three amplitudes are equal, $\phi = 120°$, and $\theta = 240°$.

The best experimental approximation to a pure traveling sinusoidal magnetic field and the best phase relations for the exciting currents were obtained with a symmetric connection of the coils [10,11]. In this case the coil at each end and the two central coils from each stator were connected to the same phase, with the coils from the two stator cores in parallel. The resulting coil currents for the generator, since the upper and lower core slots alternate, are thus $-I_A$ in coil sides (slots) 0 and 1 (numbering from 0 to 23 to correspond to the definition of n), $+I_B$ in coils 2 through 5, $-I_C$ in coils 6 through 9, $+I_A$ in coils 10 and 11, and then the negative of the preceeding currents in 12 through 23.

The total magnetic flux density for all three phases without any fluid present or slot effects included is

$$\begin{aligned} B_E = \frac{\mu_o N}{2\pi g} \sum_{m=1}^{\infty} \Bigg\{ & \frac{I_a}{m} \Big[A_1[\cos(m\xi x + \omega t) + \cos(m\xi x - \omega t)] \\ & + A_2[\sin(m\xi x + \omega t) + \sin(m\xi x - \omega t)] \Big] \\ & \frac{I_b}{m} \Big[B_1[\cos(m\xi x + \omega t - \phi) + \cos(m\xi x - \omega t + \phi)] \\ & + B_2[\sin(m\xi x + \omega t - \phi) + \sin(m\xi x - \omega t + \phi)] \Big] \\ & \frac{I_c}{m} \Big[C_1[\cos(m\xi x + \omega t - \theta) + \cos(m\xi x - \omega t + \theta)] \\ & + C_2[\sin(m\xi x + \omega t - \theta) + \sin(m\xi x - \omega t + \theta)] \Big] \Bigg\}; \end{aligned} \tag{3.10}$$

where $$A_1 = F_s(0) + F_s(1) - F_s(10) - F_s(11), \tag{3.11a}$$

$$A_2 = -F_c(0) - F_c(1) + F_c(10) + F_c(11), \tag{3.11b}$$

$$B_1 = -\sum_{n=2}^{5} F_s(n), \tag{3.11c}$$

$$B_2 = \sum_{n=2}^{5} F_c(n), \tag{3.11d}$$

$$C_1 = \sum_{n=6}^{9} F_s(n), \tag{3.11e}$$

$$C_2 = -\sum_{n=6}^{9} F_c(n), \tag{3.11f}$$

$$F_s(n) = \sin[m\xi(d+(n+12)\delta)] - \sin[m\xi(d+n\delta)], \tag{3.12a}$$

and

$$F_c(n) = \cos[m\xi(d+(n+12)\delta)] - \cos[m\xi(d+n\delta)]. \tag{3.12b}$$

The final step in calculating the field without the fluid and slot effects is to include the finite width of the coil. In the above the coil width has been considered to be an impulse. To include the finite coil width a five-point average of the field given by Eq. 3.10 is taken in the numerical evaluation to convert the steps in the field at each slot to jumps with a non-infinite slope.

3.2.3 Finite-Width Slots

The effect of the slots in the iron cores for the coil sides is to decrease the magnetic flux density under each slot. This is taken into account in the analysis by multiplying the field given by Eq. 3.10 by a modulating function due to the increased air-gap length. The slot effect will depend on where between the two cores the field is measured or calculated. Here attention is confined to the center line of the channel where the modulating functions for the slots in both cores are equal.

The trial modulating functions were chosen because they had approximately the correct shape as determined by Carter [12]. The first function tested was a gaussian density, but a computer solution proved to be impractical. Thus a sinusoidal function was used with the arguement adjusted so that the modulation due to each slot decreases to zero at the edge of the slot. Because the slots are wider than the teeth and thus overlap slightly, the total modulating function is always less than unity except outside of the slots at the ends of the stator.

The modulating function chosen is

$$f(x) = \prod_{n=1}^{23} [1 - \alpha f_1(x,n)] \tag{3.13a}$$

where

$$f_1(x,n) = \begin{cases} \cos[\pi(x-d-n\delta)2w], & |x-d-n\delta| < w \\ 0, & |x-d-n\delta| > w \end{cases} \tag{3.13b}$$

w is the slot width, and α is the modulation amplitude. The resulting expression for the total empty-channel magnetic flux density is

$$B_{ET} = f(x)B_E \tag{3.14}$$

where B_E is given by Eq. 3.10.

The modulation amplitude was obtained experimentally by matching the average values of the experimental field and the theoretical field as given by Eq. 3.14 for the same exciting current amplitudes and phase angles. The value of α obtained, 0.16, corresponds to a Carter coefficient of 1.22. This is very close to the value of 1.20 used in the generator design for the actual ratio of slot width to air-gap length [1].

The peak magnetic flux density measured with a 20-turn $\frac{1}{4}$-inch-diameter pick-up coil is shown in Fig. 3 for 40 amps per phase, current phase angles of -127.3°, and $+129.8^\circ$, and no channel or fluid. Measurements were made every 1/16 inch. The calculated field using the measured exciting current amplitudes and phase angles, also shown in Fig. 3, agrees well with the measured field. The calculated field is shown as it would be measured by the same pick-up coil. The calculated field is larger near the ends of the stator because of the neglected fringing, and this also has an effect away from the ends because of the zero-average field condition used for each coil.

3.3 FLUID-FLUID INTERACTION

The empty-channel magnetic flux density will be attenuated and shifted in phase by the addition of the fluid. One advantage of the Fourier series approach is that the effect on each component of the Fourier series is already known [1]. The amplitude is multiplied by $[1 + (sR_M 2a_f/g)^2]^{-\frac{1}{2}}$ and the phase is shifted by $\arctan(sR_M 2a_f/g)$. The factor $2a_f/g$ appears in both expressions because that is the fraction of the total air gap occupied by the fluid. Here $s = (v_s - v)/v_s$ is the fluid slip, v_s and v are the magnetic field and fluid velocities, and R_M is the magnetic Reynolds number. Both v_s and R_M are functions of the field harmonic m, and are given by

$$v_s = \omega L/2\pi m \tag{3.15}$$

and

$$R_M = \mu_o \sigma_f v_s L/2\pi m , \tag{3.16}$$

where σ_f is the electrical conductivity of the fluid. The total stator length, L, rather than the fundamental wavelength, λ, is the appropriate length.

The magnetic flux density with the fluid present is given by

$$B_T = f(x)\,\frac{\mu_o N}{2\pi g}\sum_{m=1}^{\infty}\frac{1}{[1+(sR_M 2a_f/g)^2]^{\frac{1}{2}}}\left\{\frac{I_a}{m}\left[A_1[\cos(m\xi x-\psi+\omega t)+\cos(m\xi x-\psi-\bar{\omega}t)]\right.\right.$$
$$\left. + A_2[\sin(m\xi x-\psi+\omega t)+\sin(m\xi x-\psi-\omega t)]\right]$$
$$- + \frac{I_b}{m}\left[B_1[\cos(m\xi x-\psi+\omega t-\phi)+\cos(m\xi x-\psi-\omega t+\phi)]\right.$$
$$\left. + B_2[\sin(m\xi x-\psi+\omega t-\phi)+\sin(m\xi x-\psi-\omega t+\phi)]\right]$$
$$+ \frac{I_c}{m}\left[C_1[\cos(m\xi x-\psi+\omega t-\theta)+\cos(m\xi x-\psi-\omega t+\theta)]\right.$$
$$\left.\left. + C_2[\sin(m\xi x-\psi+\omega t-\theta)+\sin(m\xi x-\psi-\omega t+\theta)]\right]\right\}, \qquad (3.17)$$

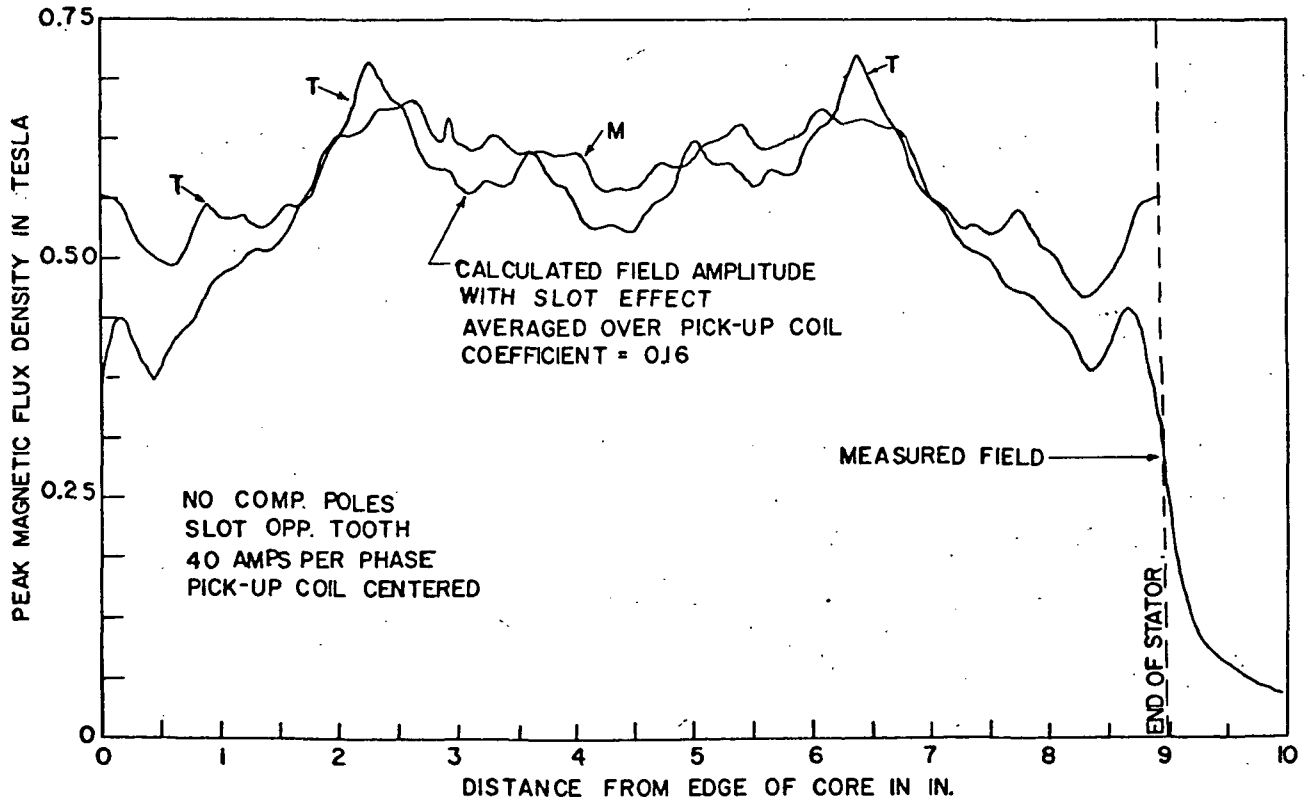

Fig. 3. Measured and calculated peak magnetic flux density amplitudes for symmetrical wye-connected excitation.

where

$$\psi = \arctan(sR_M 2a_f/g) \tag{3.18}$$

and the coefficients are given by Eqs. 3.11 and 3.12. For the experimental generator, the addition of the fluid has little effect on the magnitude and causes a small phase shift.

3.4 POWER

The powers are calculated from the Fourier series terms by using the power-flow formulas [1,3] for each magnetic-field term in the series with the correct slip and magnetic Reynolds number. The power contribution from each term is orthogonal, so that superposition of the powers can be used. This is one major advantage of the Fourier series technique. The calculated magnetic flux density with the fluid present, the net electrical input power, the net mechanical output power, and the ohmic loss in the fluid are listed for the first three harmonics (m = 1 through 3) or six terms of the series in Tables IV to VI for three experimental data points. The electrical and mechanical powers are negative for generator operation, and excitation and viscous losses are not included. The negative harmonics are fields traveling in the direction opposite to the fluid. Note that the fundamental (+1) makes the major contribution to the totals powers, but that the other harmonic contributions become relatively larger at the smaller slip values desired for high-efficiency generator operation. As the slip based on the fundamental approaches zero, the fundamental powers approach zero but the other terms change little. For the s =-0.24 case, Table IV, the harmonic contribution to the ohmic fluid loss is equal to that for the fundamental, but the percentage contribution to the other powers is smaller. The harmonic contributions change relatively little with the fundamental slip, but their percentage contribution is less for the higher-slip cases listed.

The measured and calculated net electrical powers are compared in Table VII for five data points, where the estimated ohmic coil loss has been removed from the measured power. The differences between the two are substantial, indicating that refinements in the calculations are needed. The discrepancy is largest at the smallest slip value, as expected. Note that core, side-bar, and velocity-profile losses are not included in the calculated powers.

3.5 DISCUSSION

Improvements in the existing Fourier series approach have not been fruitful because some of the basic assumptions are not good. Rather than make minor improvements it was decided to revise the procedure. The magnetic field due to the current in a single slot is calculated first, including the effects of the slots and the fringing due to the finite stator length on the magnetic field before applying the zero-average magnetic flux condition. If this is not done in the proper order the amplitudes obtained will be incorrect, and this is particularly important for slots located near the ends of the stator. A single slot is chosen rather than a pair because then various methods of grading the exciting

current may be evaluated theoretically. Superposition is used to obtain the total magnetic field without the fluid. The effect of the fluid on the magnetic field and the resulting powers are then obtained as above. This technique is presently under development for the experimental generator, but it may be applied to any linear induction machine.

Table IV. Fourier Series powers for 20 amps per phase, s = -0.24, and current phase angles of -131.5° and 128.4°

Harmonic	Magnetic Flux Density	Net Elec. Input Power	Net Mech. Input Power	Fluid Ohmic Loss
+1	0.277	-643	-795	152
-1	0.019	30	-37	67
+2	0.026	-9	-22	13
-2	0.009	3	-6	9
+3	0.018	-3	-13	9
-3	0.010	2	-7	9
TOTAL		-621	-919	298

Table V. Fourier Series powers for 20 amps per phase, s = -0.74, and current phase angles of -132.7° and 129.7°

Harmonic	Magnetic Flux Density	Net Elec. Input Power	Net Mech. Input Power	Fluid Ohmic Loss
+1	0.235	-1450	-2530	1070
-1	0.020	38	-66	104
+2	0.024	-13	-45	32
-2	0.009	3	-11	14
+3	0.018	-5	-27	22
-3	0.010	3	-14	16
TOTAL		-1420	-2760	1340

Table VI. Fourier Series powers for 20 amps per phase, s = 0.41, and current phase angles of -130.9° and 126.7°

Harmonic	Magnetic Flux Density	Net Elec. Input Power	Net Mech. Input Power	Fluid Ohmic Loss
+1	0.267	1030	608	426
-1	0.015	13	-8	21
+2	0.027	-1	-1	0
-2	0.009	2	-2	4
+3	0.018	-1	-2	1
-3	0.010	1	-2	3
TOTAL		1050	585	464

Table VII. Comparison of measured and calculated net electrical input powers.

Fluid Velocity	Slip	Net Electrical Input Power, Watts	
		Measured	Calculated
4.4	0.68	2020	1430
8.0	0.41	1720	1050
16.9	-0.24	765	-621
18.6	-0.36	450	-909
23.8	-0.74	-480	-1420

SECTION IV

EXPERIMENTAL DATA

4.1 INTRODUCTION

Concurrently with developing an improved analytical model, the experimental data is being processed for consistency and correlations. As described in the introduction, there are roughly 200 data points for a variety of excitation conditions, both with and without the compensating poles. All data obtained to date has been transferred to IBM cards, and is available to others developing analytical models. (With the present emphasis on analysis, data exchange on the existing experiments should be encouraged.) Each data point consists of 22 cards containing 143 to 196 numbers, depending on the case, for the terminal voltage and current magnitudes and phase angles, the powers, the 38 magnetic-field monitoring-coil voltages, pressures, etc. It requires at least twenty minutes for one data run, but generator operation is reasonably constant over the time period.

The data sheet for the data point 20-4-28 is shown in Fig. 4, and the computer printout of the data in Fig. 5. The zeros on card 12 are where the data for the self-excited operations is entered. The case shown is for operation connected to the power line and with the compensating poles present.

Checking the data for consistency involves utilizing the built-in redundency among some of the data, double measurements, and plotting data to eliminate obvious errors. Some errors have been detected, but the overall results have been very good. As an example, particular difficulty during operation was experienced with the phasemeter. This is a key instrument, not needed for dc, because without phase data it is impossible to reconstruct the magnetic field from the exciting currents or from the magnetic-field monitoring-coil measurements. It has been necessary to correct some data for a 180^{o} inconsistency of the instrument, but otherwise most results have checked within $\pm 2^{o}$ between the readings, the built-in redundency, and the power calculations except for a few obvious errors or cases where the instrument would not yeild a reading. From the total set of data points only a few have been rejected as incomplete or inconsistent, plus some early cases where the measurements indicated the strong possibility of a two-phase mixture in the generator [11].

The measured and calculated phase angles for the data point 20-4-28 are shown in Table VIII. The first three angles are the voltage-current angles for the three phases, the others are the angles between the line voltages. The calculated angles use either the redundency or the power factors.

4.2 OPERATION CONNECTED TO THE POWER LINE

Data points were measured for various terminal conditions and excitation currents between 20 and 40 amps per phase. Attention is confined here to the results for 20 amps because higher fluid velocities could be attained. Also pump operation at higher currents was limited due to excessive vibration and/or cavitation. The powers and efficiency are increased for higher

Fig. 4. Data Sheet for Data Point 20-4-28.

INDUCTION GENERATOR DATA - WITH FLOW

20-4-28

CASE: 4YS-CP EXCITED

DATE: 4-6-71-(4)

NOTES:

DATA BY:

MAIN WINDING EXCITATION

ALL PHASE ANGLES REL. TO I_1, UNLESS IND. (USE YEL. TER. FOR ϕ_V, CT FOR ϕ_I)

I_1 20 I_2 20 I_3 20 CT TAP 25.5

V_{1N}	V_{2N}	V_{3N}	
			(Weston)
92.7	100.7	101.2	(OVM)
V_{12}	V_{23}	V_{31}	(Weston)
164.5	177.8	167.2	(OVM)

Voltm. R W1 107½ W2 92 W3 121½ MULT. 5 SIGNS ± F G

ϕ_{I2} −1.20 ϕ_{I3} 119.8

ϕ_{V1N} 74.2 ϕ_{I2-V2N} 76.8 ϕ_{I3-V3N} 73.6

ϕ_{V2N} −43.2 ϕ_{V3N} −166.5

ϕ_{V1V2} −117.4 ϕ_{V1V3} −61.1 (5) ϕ_{V2V3} −123.6

V_{ee} 263 ϕ_{ee} −119.0

COMPENSATING POLES EXCITATION

I_1 17.3 — I_3 22.4 —

ϕ_{I1} 21.6 ϕ_{I3} −59.1

V_{1N} 104.5	V_{2N} 28.2	V_{3N} 73.0	V_{4N} 107.3
V_{12} 114.8 —		V_{34} 155.5 —	
W_1 159	W_2 —	W_3 72	W_4 —

ϕ_{V1} 74.3 ϕ_{V2} −32.9 ϕ_{V3} 75.5 ϕ_{V4} −166.6

MULT. 5 SIGNS ± ϕ_{V12} 87.6 ϕ_{V34} 37.5

SENSE COIL MEASUREMENTS

UPPER CORE

V	1.562	2 1.222	3.741	4 1.170	5 1.539	6 1.475	7.804	8.776	9.771	10.693
ϕ	80.4	128.8 (5)	−107.8	−29.8	17.4 (5)	−121.9	16.6	−104.3	140 (5)	139.7
V	11.697	12.466	13.449	14.346	15.432	16.330	17.384	18.0056	19.743	
ϕ	19.5	50.6 (5)	76.6	−8.5	17.5	47.2	−41.2	140	48.1 (5)	

LOWER CORE

V	0.717	2 1.524	3.906	4.778	5 1.241	6 1.273	7 1.480	8.241	9.807	10.834
ϕ	−29.3	19.2	1.073 (5)	16.4	128.1 (5)	109.9	−121.6	−95.3	−38.1	18.0 (5)
V	11.759	12.407	13.419	14.362	15.454 (5)	16.360	17.501	18.0061	19.779	(6) 1.543
ϕ	142.5	−42.7	−108.0	−31.5	128.0	92.0	9.1 (5)	—	113.6	−10.6

COMPENSATING POLES

V	17.956	1 1.085	27 1.069	29 1.165	37 1.359	39 1.429	47 1.394	49 1.450	
ϕ	−92.5	96.9	83.8	83.6	41.5	87	−138.8	−137.9	

FLOW DATA

INITIAL	16.5 / 16.4	P2 15.3	P3 17.8	P4 22.0	P5 18.1	P6 23.1 / 22.8	P7 17	−.140	±.01
FINAL	16.8	15.6	17.8	22.0	18.1	23.0	17	−.141	±.01
NO-FIELD	23.1	22.8	20.7	18.4	17.9	28.6	17.3	−.142	±.01

FLOW (IN) ± .01

TEMPS INT TR-N 102 TRS 102 EL 109.5 EXT TR-N 102 TRS 102 EL 114

1	20-4-28		25	4/6/71								
2	20.0	20.0	20.0	92.7	100.7	101.2	164.5	177.8	167.2	107.5	92.0	121.5
3	-120.0	119.8	74.2	76.8	73.6	-43.2	-166.5	-117.4	118.9	-123.6		
4	0.263	-119.0										
5	17.30	22.40	104.50	28.20	73.00	107.30	114.80	155.50	159.00	-72.00	5	
6	21.6	-59.1	-127.2	-54.5	134.6	-107.6	74.3	-32.9	75.5	-166.6	87.6	37.5
7	16.5	15.3	17.8	22.0	18.1	23.1	17.0	-0.40				
8	16.4	15.3	17.8	22.0	18.1	22.8	17.0	-0.40				
9	16.8	15.6	17.8	22.0	18.1	23.0	17.0	-0.41				
10	23.1	22.8	20.7	18.4	17.9	28.6	17.3	-0.42				
11	102.0	102.0	109.5	102.0	102.0	114.0						
12	0.0	0.0	0.0	0.0	0.0	0.0	0.0	0.0	0.0	0.0		
13	1.5620	80.4	1.2220	128.8	0.7410	-107.8	1.1700	-29.8	1.5390	17.4		
14	1.4750	-121.9	0.8040	16.6	0.7760	-104.3	0.7710	14.0	0.6930	139.7		
15	0.6970	19.5	0.4660	50.6	0.4490	76.6	0.3460	-8.5	0.4320	17.5		
16	0.3300	47.2	0.3840	-41.2	0.0056	140.0	0.7430	48.1	0.0	0.0		
17	0.7120	-29.3	1.5240	19.2	0.9060	107.3	0.7780	16.4	1.2410	128.1		
18	1.2730	109.9	1.4800	-121.6	0.7410	-95.3	0.8070	-38.1	0.8340	18.0		
19	0.7590	142.5	0.4070	-42.7	0.4190	-108.0	0.3620	-31.5	0.4540	128.0		
20	0.3600	92.0	0.5010	9.1	0.0061	0.0	0.7790	113.6	1.5430	-101.6		
21	0.9560	-97.5	1.0850	96.9	1.0690	83.8	1.1650	83.6	1.3590	41.5		
22	1.4290	43.7	1.3240	-138.8	1.4500	-137.9	0.0	0.0	0.0	0.0		

Fig. 5. Computer Printout of Data Point 20-4-28.

phase currents, but the qualitative behavior is the same.

The net electrical input power to the fluid (gross electrical input power minus excitation loss) for the first 79 data points at 20 amps per phase without the compensating poles is plotted versus fluid velocity in Fig. 6. The first 18 data points (triangles) were measured before adding more NaK to the flow system. The evidence indicates that for these cases the working fluid was a mixture of liquid and vapor, so that the venturi used to measure the fluid velocity read low. (The static pressure is much less in the generator than in the venturi, so that the mixture expands in the generator.) The next 46 points (squares) were measured after adding more NaK. The last 15 data points (circles) correspond to a change in the technique used to measure the fluid velocity which is more accurate at low velocities. Each group is quite consistent within itself for an experiment. The data is now being corrected for the velocity measurements. In this fashion data that would otherwise be lost is utilized.

At zero slip, 12.6 m/sec, there is a significant discrepancy from zero net power. This is probably due to end effects, the copper side bars, the fluid velocity profile, the slot harmonics, and the poor current phase angles (around 10^{o} off from $\tilde{}120^{o}$). The improved computer program will eventually help to resolve the source of this discrepancy. (See Table VII.)

Data points were also measured with the end coils on each stator shorted to reduce the magnetic flux through the end teeth, or in a sense to allow the generator to provide its own compensation. This case does not appear to be attractive because the slope of the power versus velocity curve is reduced from that for the previous case, or there is less useable power. This was also true for self-excited operation.

The generator was also operated with the compensating poles installed for a variety of terminal conditions. Data was taken first with the compensating windings open circuited and short circuited, as this will be useful in determining the characteristics of the poles and their interaction with the main winding. It was not possible to pick an optimum setting for the magnitude and phase of the compensating-pole currents, as adjusting them for maximum power lead to inbalances between the three main current phase angles, while balancing the phase angles unbalanced some other quantity. Further analysis of the data is required to understand the operation of the compensating poles with this generator and the optimum setting of their excitation.

Table VIII. Angle checks for data point 20-4-28.

Measured	Calculated	
	From other Angles	From Power
74.2		73.2
76.8	76.8	76.8
73.6	73.7	72.5
-117.4	-117.4	
118.9	119.3	
-123.6	-123.3	

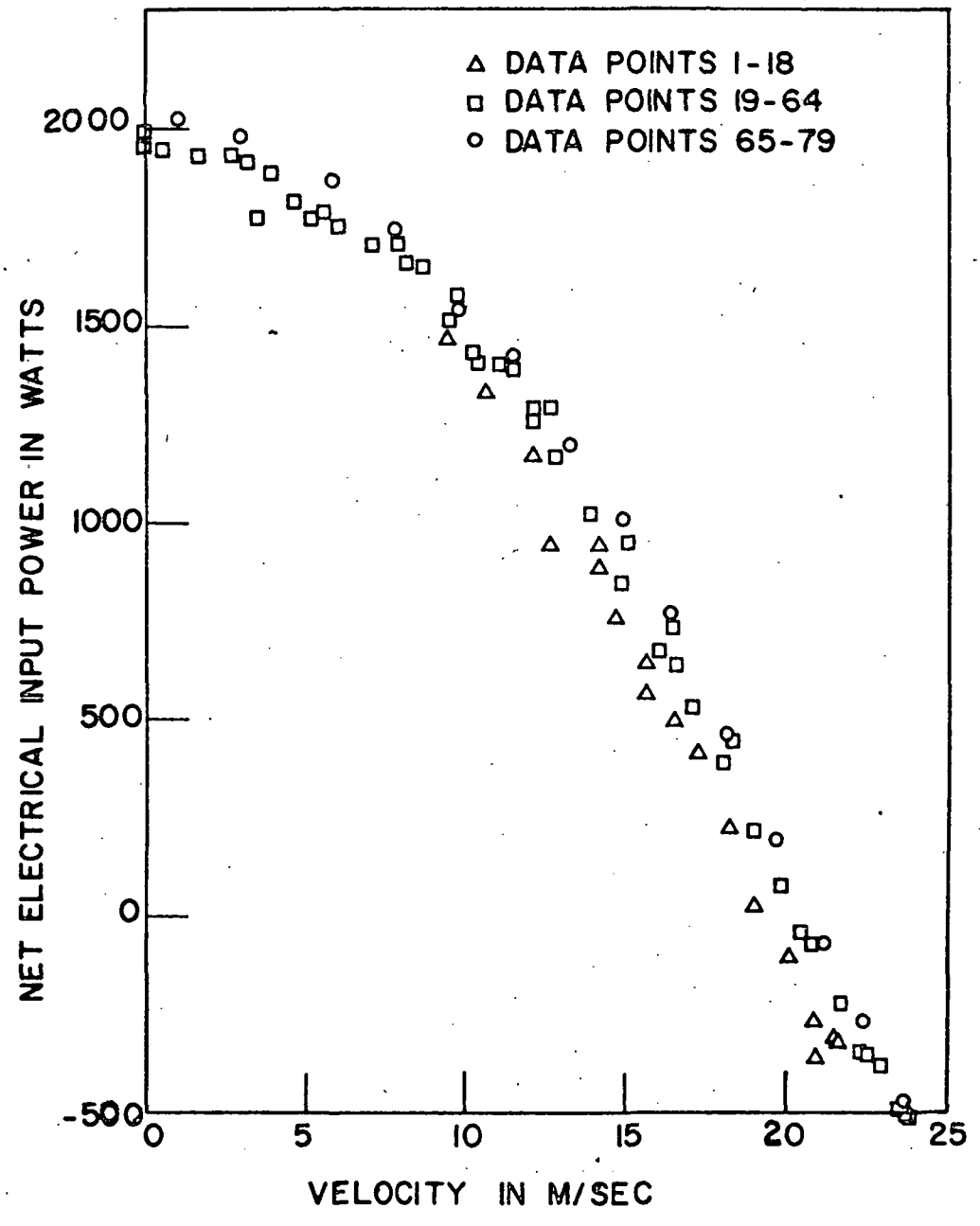

Fig. 6. Net electrical input power versus fluid velocity for 20 amp per phase data points.

4.3 SELF-EXCITED OPERATION

The generator will operate in the self-excited mode, no connection to the power line, with capacitance connected across the terminals to supply the required reactive power. The generator then operates as an oscillator producing net output power at the frequency determined by the generator inductance and the external capacitance. The main points noted were:

1. Operation is very stable, and there is no trouble with fluctuations.
2. The generator starts, even after several days, without any external trigger. All that is required is external capacitance and a fluid velocity sufficiently above the field velocity determined by the capacitance.
3. The frequency is controlled by the external capacitance, with a frequency change from no load to full load at a given capacitance value of only a few tenths of a hertz.
4. The generator is short-circuit safe because it loses its excitation, and restarts upon removal of the short. The variation in output voltage with load may be decreased by adding capacitance in series with the load, although this was not tested.
5. Operation appears to be better self-excited, probably because the generator adjusts the current phase angles to minimize the losses or optimizes the performance within the terminal constraints. The generator appears able to do this better than an external operator or control system.

The external capacitance on the three phases could be adjusted to balance the phase currents, but the powers for the phases were not balanced, as occurred for normal line operation, and optimizing the output power required different load resistances for the three phases. The fluid velocity or slip varied with the generator load but was almost independent of the control valve, provided that self-excited operation could be maintained. The start of self-excited operation is not instantaneous, but requires a few seconds before anything happens.

The known external capacitance C of the generator and the frequency f can be used to calculate the equivalent inductance L of the three phase in parallel from the conventional oscillator equation

$$f = \frac{1}{2\pi\sqrt{LC}} \qquad (4.1)$$

The inductance is about 4.7 millihenries without the compensating poles, and is constant over the 35 to 60 hertz frequency range tested. This is about twice the inductance calculated from the stored magnetic energy in the air gap between the stators. The difference must be due mainly to the leakage flux.

According to Eq. 4.1 the plot of log C versus log f should be a straight line. This is shown in Fig. 7 for operation without the compensating poles. The slight spread over frequency at a single capacitance value is due to the slight change in frequency with load or output power and fluid velocity. For example, the spread around log f = 3.92 is from 50.4 to 50.9 hertz, or one percent.

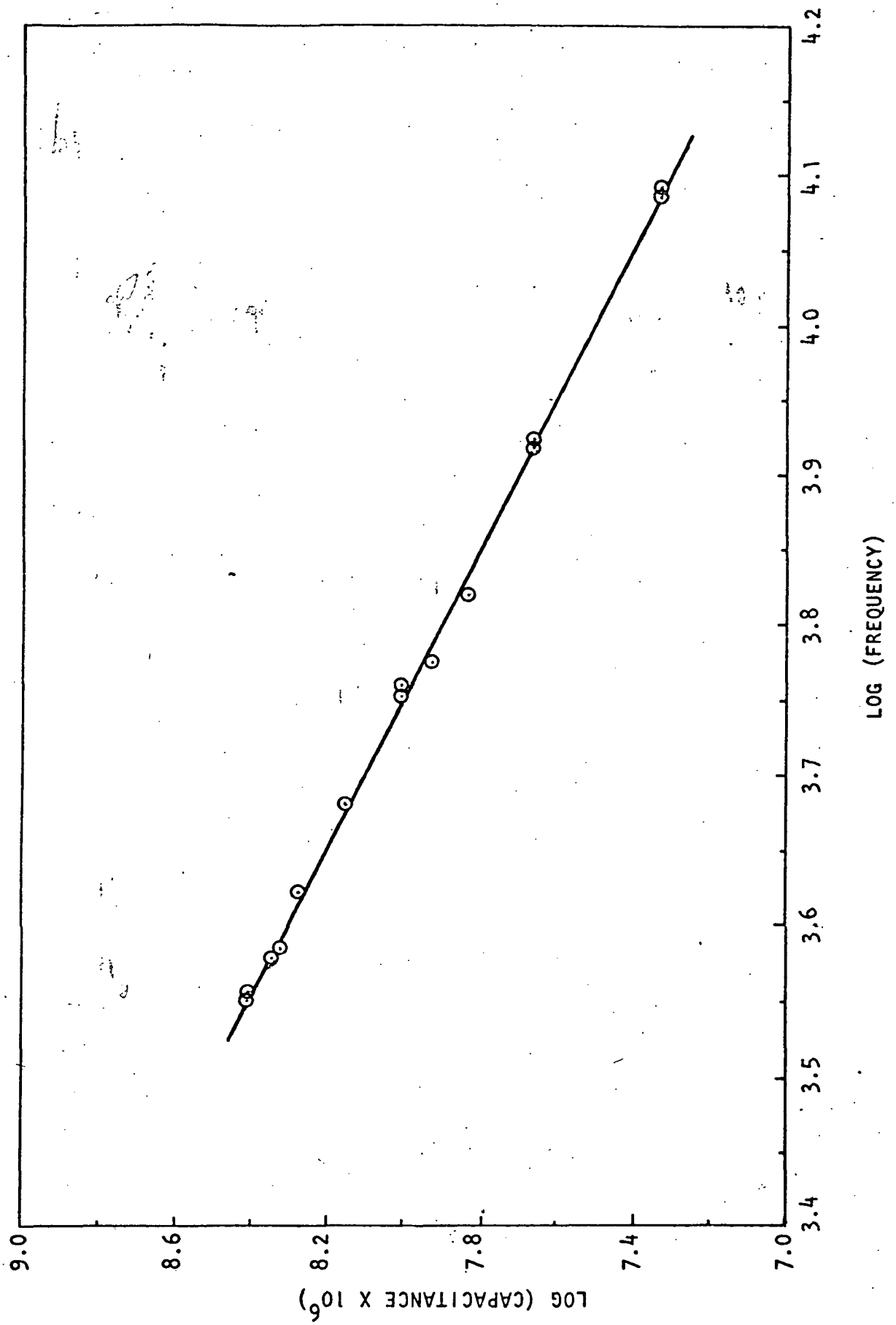

Fig. 7. Log (capacitance x 10^6) versus Log (frequency) for self-excited data points without compensating poles.

Seven data points have been obtained with the compensating poles installed and excited. It was not possible to draw any conclusions from these because of the difficulty in defining the optimum settings, as discussed in Section 4.2 for operation connected to the power line. More study of the compensating pole operation is required.

SECTION V

CONCLUSIONS AND RECOMMENDATIONS

A considerable amount of experimental data has been accumulated for this experimental MHD induction generator. The data is internally consistent, but interpretation of it is restricted due to the limitations of the existing analytical model.

The Fourier series analysis of the generator described in Section III appears to be promising once the required changes in the procedure are included. The available method is interesting but not accurate enough for practical use.

This research program on the MHD induction generator should be extended in two parallel paths. First the Fourier series model must be revised, and then compared against the existing data. An accurate analysis technique is needed to interpret and fully utilize the existing data. Second, there are several further experiments to perform with the existing stator before the design and construction of a new stator. Additional study of end loss and compensation methods is needed, particularly further data with the compensating poles excited. Also tests have never been performed with the channel with vanes under the compensating poles to suppress end currents due to leaks in the channel, and these tests are very important. Finally, a series of studies on a two-phase working fluid using the same stator is an important corollary to the above program as this will allow the comparison of the single- and two-phase results without the complication of a different generator structure.

SECTION VI

NEW TECHNOLOGY

No new technology items have been identified in connection with this program.

REFERENCES

1. Pierson, E.S., Brown, G.A., and Jackson, W.D., Liquid Metal Magnetohydrodynamics, AFAPL-TR-69-33, Air Force Aero Propulsion Laboratory, Air Force Systems Command, Wright-Patterson Air Force Base, Ohio, May 1969.

2. Discussion for Section 2-d, Design and Performance Studies, Electricity from MHD, 1968, International Atomic Energy Agency, Vienna, 1968, Vol. VI, 3709.

3. Pierson, E.S., The MHD Induction Machine, Sc.D. Thesis, Department of Electrical Engineering, Massachusetts Institute of Technology, Cambridge, Massachusetts, September 1964; or AFAPL-TR-65-107, Research Laboratory of Electronics, Massachusetts Institute of Technology, Cambridge, Massachusetts, May 1966.

4. Elliott, D.G., private correspondence.

5. Pierson, E.S., and Jackson, W.D., Channel Wall Limitations in the MHD Induction Generator, ANL-7148, Argonne National Laboratory, Argonne, Illinois, March 1966.

6. Moody, L.F., "Friction Factors for Pipe Flow," Trans. Amer. Soc. Mech. Engrs., 66, 671, 1944.

7. Cerini, D.F., and Elliott, D.G., "Performance Characteristics of a Single-Wavelength Liquid-Metal MHD Induction Generator with End-Loss Compensation," Proceedings of the Eighth Symposium on Engineering Aspects of Magnetohydrodynamics, Stanford, California, 1967, p. 11.

8. Moszynski, J.R., Reduction of Electrical End Losses in MHD Generator Channels by Insulating Vanes, ANL-7188, Argonne National Laboratory, Argonne, Illinois, 1967.

9. Elliott, D.G., "Numerical Analysis Method for Linear Induction Machines," Proceedings of the Twelfth Symposium on Engineering Aspects of Magnetohydrodynamics, A.N.L., Chicago, Ill., March 1972, pp. IV.3.1 - IV.3.9.

10. Pierson, E.S., Magnetohydrodynamic Induction Generator Experimental Study, Final Technical Report for Contract No. 952453, Jet Propulsion Laboratory, Pasadena, California, N70-29169, April, 1970.

11. Pierson, E.S., "Preliminary Experimental Results from a One-Wavelength MHD Induction Generator," Proceedings of the Eleventh Symposium on Engineering Aspects of Magnetohydrodynamics, C.I.T., Pasadena, Cal., 1970, pp. 161-164.

12. Alger, P.L., The Nature of Induction Machines, Gordon and Breach, New York, 1965, p. 165.